Simple Constitutive Equations for Steel at High Temperature

PATRICK F. KOZLOWSKI, BRIAN G. THOMAS, JEAN A. AZZI, and HAO WANG

This work develops and investigates simple unified constitutive equations to model the mechanical behavior of plain carbon steel in the austenite temperature region for use in finite element stress analysis of processes such as continuous casting. Four different forms of constitutive relations are considered: constant structure, time-hardening, strain-hardening, and simultaneous time- and strain-hardening models. Each relation is judged on its ability to reproduce experimental data from both tensile and creep tests and its ability to exhibit reasonable behavior under complex loading conditions. Three of the equations appear suitable for small strain monotonic loading conditions for a wide range of low strain rates (10^{-3} to 10^{-6} s^{-1}), high temperatures (950 °C to 1400 °C), and varying carbon contents (0.005 to 1.54 wt pct C).

I. BACKGROUND

THE recent increases in computational speed and availability of finite element software are making stress analysis of casting processes feasible and desirable. A major obstacle to accurate mathematical analysis is finding and evaluating material constitutive equations that adequately describe the complex relationship that exists between stress, strain, and time at elevated temperatures. These equations should characterize mechanical behavior of the metal under the conditions encountered during the process. Choices include time-independent elastoplastic relationships, elastoplastic models with creep, unified models with evolving internal state variables, and elasto-viscoplastic models. Each of these approaches has both merits and problems.

Assuming stress, σ, is caused solely by elastic strain, ε_e, the rate forms of the constitutive equations for an isotropic material in uniaxial loading are

$$\dot{\sigma} = E\dot{\varepsilon}_e \quad [1]$$

$$\dot{\varepsilon} = \dot{\varepsilon}_e + \dot{\varepsilon}_p + \dot{\varepsilon}_T \quad [2]$$

where the symbols are defined in the Nomenclature at the end of the article.

Integrating these equations under the appropriate boundary conditions produces the deformation history (stress-strain-time response) of the material under any arbitrarily chosen loading conditions. These loading conditions could range widely and include the limiting cases defined in standard tensile tests (imposed constant total strain rate), creep tests (imposed constant stress), and stress relaxation tests (imposed constant total strain).

In a typical casting, every point in the material experiences a different complex loading history, which usually varies greatly as time progresses. To perform the required multidimensional analysis, the effective (uniaxial) applied stress and strain needed in Eqs. [1] and [2] are usually determined from their spatial components using a von Mises criterion.[1] The equations are then solved using the finite element method, which simultaneously calculates incremental changes in stress and strain at each location in the solid and at each time step during the simulation, under these complex loading conditions.[2] In doing this, the increments of inelastic strain are decomposed into their spatial components in proportion to the deviatoric stresses using the Prandtl-Reuss equations.[1]

Inelastic strains are induced by the stresses, or elastic strains, which arise in response to the loading conditions. In many casting processes, small differences in the thermal strains, ε_T, constitute a significant fraction or even all of the load. The total strain is often constrained to be constant, so the extent of the induced inelastic strain, in turn, directly affects the elastic strains and the loading history. Because of this coupling, the constitutive equations have a magnified influence on the predicted stress in casting processes.[3] It is therefore important to find general constitutive equations that are accurate for the range of mechanical conditions encountered.

Elastoplastic constitutive equations have been used to model many processes, including continuous casting.[4,5,6] This is because the numerical methods for integrating the equations over both time and position are well established and robust. However, at the high temperatures encountered in casting, the mechanical properties are very sensitive to strain rate. Since casting involves wide ranges in strain rate, a time-independent elastoplastic analysis is crude.

Improving the elastoplastic approach by adding creep[7,8] leads to a more complicated analysis. Splitting the inelastic strain, ε_p, into a rate-independent plastic part and a rate-dependent creep part, as is often done, is physically arbitrary, since only the combined effect can be measured. Consequently, it is difficult to find a consistent set of elastoplastic and creep equations that, when integrated together, accurately describes the mechanical behavior of the metal under the range of conditions encountered. It is also difficult to test their accuracy. Since creep occurs during tensile tests and plastic work hardening occurs during creep tests, relations derived from either type of test are equally valid in describing the total

PATRICK F. KOZLOWSKI, formerly Graduate Student, University of Illinois at Urbana–Champaign, is Manufacturing and Systems Engineer, Caterpillar, Inc., Aurora, IL. BRIAN G. THOMAS, Associate Professor, and HAO WANG, Graduate Student, are with the Department of Mechanical and Industrial Engineering, University of Illinois at Urbana–Champaign, Urbana, IL 61801. JEAN A. AZZI, formerly Graduate Student, University of Illinois at Urbana–Champaign, is Research Engineer, Woodward Governor Company, Rockford, IL 61101.

Manuscript submitted February 5, 1991.

behavior. It is ill advised to simultaneously use creep equations and time-independent stress-strain data taken from independent sources.

Models with evolving internal "structure" variable(s) are gaining in popularity.[9,10–13] These "unified" models characterize the mechanical behavior of a given material under arbitrary loading conditions by defining its instantaneous inelastic strain-rate response in terms of "state variables" which include temperature, stress, and structure.

$$\dot{\varepsilon}_p = \dot{\varepsilon}_p(\sigma, T, \alpha_1, \alpha_2, \ldots, \alpha_n) \quad [3]$$

$$\dot{\alpha}_i = \dot{\alpha}_i(\dot{\varepsilon}_p \ldots) \quad [4]$$

These equations can accurately model the complete range of physically observed behavior, since the "structure parameters" in the model, α_i, can evolve in the same way as their associated microstructural properties that characterize the material's resistance to inelastic flow. For example, an increase in the slope of the stress-strain curve during a tensile test produced by work hardening or a decrease due to recovery can be reproduced in a model by corresponding increases or decreases to a structure parameter that represents dislocation density.

Orisamolu and Singh[14] developed a constitutive model of this form, including thermomechanical energy for large strains, using two structure variables: a strain-hardening parameter and thermoinelastic strain. The Miller model[9] also uses two structure variables, back stress and drag stress, to exhibit the effects of kinematic and isotropic hardening. Anand[10] and Brown *et al.*,[11] have demonstrated the potential for single structure-variable models using the following specific form of Eq. [3]:

$$\dot{\varepsilon}_p = \dot{\varepsilon}_p\left(\frac{\sigma}{\alpha_1}, T\right) \quad [5]$$

Smelser and Richmond[15] applied a model of this general form to model casting of aluminum.

Unfortunately, these models with evolving structure variables are generally more difficult to integrate numerically and implement into existing programs using the finite element method (FEM). They can require over two orders of magnitude more execution time than the elastoplastic methods.[16] This is likely due, in part, to the dependency of the structure variables on strain rate, which, being a derivative, is known to less accuracy than the strain or stress and is subject to wider variation during convergence iterations. This further increases the "stiffness" of the differential equations. It is also difficult to evaluate the parameters needed for these models. Many of the phenomena which benefit most from these sophisticated evolving structure parameters are related to large strains for forming processes[10,11,12,14] which are not a concern to casting.

Simple elasto-viscoplastic equations offer another alternative. When treated as unified constitutive models, equations of the following form and Eq. [1] can be used without modification to describe the complete range of mechanical behavior:

$$\text{Model I:} \quad \dot{\varepsilon}_p = \dot{\varepsilon}_p(\sigma, T) \quad [6]$$

$$\text{Model II:} \quad \dot{\varepsilon}_p = \dot{\varepsilon}_p(\sigma, T, t) \quad [7]$$

$$\text{Model III:} \quad \dot{\varepsilon}_p = \dot{\varepsilon}_p(\sigma, T, \varepsilon_p) \quad [8]$$

$$\text{Model IV:} \quad \dot{\varepsilon}_p = \dot{\varepsilon}_p(\sigma, T, \varepsilon_p, t) \quad [9]$$

Equations [6] through [9] present four possible functional forms to define the inelastic strain rate needed in Eq. [2]. In all cases, the mechanical response of a given steel during arbitrary loading conditions is assumed to be isotropic and to depend only upon the state variables of stress, temperature, and time and/or inelastic strain. This means that the material structure (for a given temperature, stress, and steel grade) is characterized solely by the scalar parameters of time since the start of loading and/or the total inelastic strain accumulated up to that time.

These equations have the advantage of being easy to implement into FEM code, and numerical methods for their evaluation are available.[17,18,19] This is because time is always known and inelastic strain always must be converged upon during every step of a nonlinear stress analysis anyway. However, since no yield surface is defined, and plastic strain can begin immediately, these methods still require more computational effort than elastoplastic methods.

For a single type of experimental data, the parameters for Eqs. [6] through [9] are relatively easy to find and can even be described using databases containing the original test data.[20] Equations of the form of Eqs. [6] and [7] are commonly derived from simple tensile or creep tests and Eq. [8] from tensile tests. Equations [6] and [7] have been used successfully by several researchers to model bulging in continuous casting.[21–27]

The worst attribute of these models is their obvious deficiency in characterizing the evolution of material structure. In general, the structure of a steel would be expected to change during a complex deformation history in ways not directly related to the time or inelastic strain. Nevertheless, models with these forms are widely used to represent the complex loading conditions encountered during casting processes that differ greatly from the test data they were based upon. It is therefore important to evaluate and optimize their performance.

The objective of this work is to develop and compare the abilities of four different elasto-viscoplastic constitutive equations, based on Eqs. [6] through [9], to quantify the mechanical behavior of plain carbon steel under conditions typically encountered during casting processes such as continuous casting:

(1) temperature range of austenite (900 °C to 1400 °C).
(2) slow strain rate (10^{-3} to 10^{-6} s^{-1})
(3) small strains (usually below 2 pct)
(4) carbon contents ranging from pure iron (0.005 pct C) to high carbon steel (1.54 pct C)
(5) complex loading histories

II. MODEL FORMULATION

Optimum versions of the simple constitutive equations, of the forms suggested in Eqs. [6] through [9], were sought to model the mechanical behavior of steel under continuous casting conditions. To accomplish this, parameters for each model were simultaneously fit to experimental tensile and creep data using the method

described in Section A. The equations were then evaluated for their ability to reproduce both the experimental data and behavior under complex loading conditions.

Each of the model formulations has several common features. First, in order to model various plain carbon steels, a quadratic function of carbon content was used as a scaling constant, C, for each of the constitutive equations. First-order interactions between carbon content, temperature, and inelastic strain were originally included in the scaling factor but were found to be negligible. Although evidence does exist showing the importance of solutes such as manganese, niobium, and phosphorus,[28] the paucity of such data prevents other solutes from being included in the models.

The second common feature of each model is the temperature dependence of most of the parameters. Initially, each parameter was chosen to be a quadratic function of temperature but was later reduced to linear, if the fit indicated there was little difference.

Finally, models II through IV were formulated to handle arbitrary changes in loading conditions by treating the expression involving the net stress exponent, n, in the following general manner:

$$\dot{\varepsilon}_p = f_1(C, T)\,|f_2(\sigma)|^{n-1} f_2(\sigma) \qquad [10]$$

This commonly used procedure enables negative inelastic strain rates to arise naturally while ensuring that negative numbers are not raised to fractional powers.

A. *Parameter Estimation*

The best parameters for each model were found by minimizing the total error in matching both experimental tensile and creep data. For a given set of model parameters, the constitutive equations (Eqs. [1] through [3]) were integrated under conditions corresponding to each of the available stress-inelastic strain curves for the tensile test data and strain-time curves for the creep data. Thermal strain rate, $\dot{\varepsilon}_T$, was always set to zero, because all of the experimental data was isothermal. Integration of each curve involved a backward Euler iteration scheme within each time step to converge upon the inelastic strain rate.[29,30] A constant time step size of 0.01 to 0.7 seconds was employed for runs at low strain rates, with the smaller time steps needed for models III and IV. The time step was reduced 10 times at higher strain rates (above 10^{-3} s^{-1}). Numerical stability was not a problem for reasonable values of the parameters.

The total error between points on the model-predicted curves and corresponding points on the experimental curves was defined by the following least-squares criterion:

$$\text{Total Error (MPa)}^2 = E_1 + \frac{E_2}{(0.3)^2}$$

$$E_1\,(\text{MPa})^2 = \sum_{i=1}^{83} \sum_{j=1}^{6 \text{ or } 7} (\sigma_{ij} - \hat{\sigma}_{ij})^2$$

$$E_2\,(\text{pct m/m})^2 = \sum_{k=1}^{12} \sum_{l=1}^{7} (\varepsilon_{kl} - \hat{\varepsilon}_{kl})^2 \qquad [11]$$

In calculating the error E_1, j represents a discrete point on an individual stress-strain tensile test curve i, σ is the experimental stress, and $\hat{\sigma}$ is the predicted stress. A similar correspondence holds for E_2, which defines the total error in the estimate of the strain-time creep test curves. The constant 0.3 represents a somewhat arbitrary conversion factor between stress and strain (*i.e.*, 0.3 pct m/m = 1.0 MPa) to allow comparison of the different units. This particular value, however, weights the error more heavily toward E_1; hence, the tensile data are fitted more closely. Choosing a different value than 0.3 for this conversion factor would allow different weighting between the creep and tensile data, ranging from fitting only the tensile data to fitting only the creep data.

The simplex method for nonlinear optimization[31] was used to estimate the optimal values of the model parameters that minimize the total error in Eq. [11]. The "simplex" is a geometrical figure consisting, in N dimensions for the N model parameters, of $N + 1$ vertices and the associated edges, faces, *etc.* The method is started with an initial simplex and the error associated with each vertex. A reasonable starting value for each model parameter that could generate stable curves was found through trial and error. Starting values for the other vertices were obtained simply by perturbing these values by ±5 pct. The parameters were not normalized, so the shape of the simplex changed greatly as the search progressed.

Each step to reduce the error involves reflecting the point with the largest error through the face containing the smallest error. This requires reintegration of each of the 83 tensile and 12 creep curves, which took approximately three minutes on a dedicated Silicon Graphics Iris 4D/25. A reasonable estimate of the optimum parameter values typically required about 500 simplex steps or one day of CPU time. Convergence was defined when the error decreased by less than 1×10^{-4} MPa after any iteration. Finally, the method was restarted at this "optimum" using a ±1 pct variation in the values to define the starting simplex. This usually confirmed that the final parameter values were indeed "optimal."

Although this procedure might not be the fastest possible, it was very simple and general. Changing the form of the constitutive model was easy, because this procedure involved no evaluation of derivatives, changes to the fitting procedure, or convergence difficulties.

B. *Data*

The experimental data used in the development of the models are the tensile test data given by Wray[32] and the creep test data given by Suzuki *et al.*[33] These data were chosen over other measurements because they are both complete and comprehensive and together describe mechanical behavior over the entire strain rate, strain, carbon content, and temperature ranges of interest. In addition, these data are compatible with each other, predicting similar mechanical responses over the range of conditions where the data approximately overlap.

The 83 sets of tensile stress/inelastic strain data points were extracted directly from Table II in Wray's article[32] covering the range of conditions given in Table I of this article and including five different temperatures, six strain rates, and eight carbon contents. The data of Suzuki *et al.* was presented as a curve fit equation based on creep tests on 0.19 pct C steel.[33] Using the provided

Table I. Range of Conditions Used in Developing the Model

	From	To
Tensile tests:		
Temperature	950 °C	1200 °C
Wt pct C	0.005	1.54
Inelastic strain	0.1 pct	10 pct
Strain rate	3×10^{-3} s^{-1}	6×10^{-6} s^{-1}
Creep tests:		
Temperature	1250 °C	1400 °C
Constant stress	4.2 MPa	9.8 MPa
Time	0 s	140 s

relation, discrete strain-time data points were extracted for the given constant stress levels and temperatures and are included in Appendix I. Data for the model covered the range of conditions given in Table I.

The model was based on a temperature range where the plain carbon steel is purely in the austenite phase. This temperature range is important for continuous casting and avoids the necessity of employing mixture equations to handle multiple phases. In addition, for these strains and temperatures, primary creep is dominant. This is indicated by both the curvature of the strain-time curves and the changing positive slopes of the stress-strain curves.

It should be noted that experimental data itself has scatter. Based on the single tensile test replicated by Wray,[32] the common sample variance is estimated to be 0.0592 with 5 degrees of freedom. This implies that discrete stress points should be within ±0.27 MPa of their true values, assuming a 95 pct confidence interval for the mean. However, atypical data that do not follow the general trends are likely a greater source of scatter. This can arise from experimental problems, such as compliance of the testing equipment[10] or differences in the initial state of the test samples.[34]

The creep data are prone to similar problems. Most of the creep tests were run twice, and the time and strain at which recrystallization occurred were recorded.[35] Whenever appropriate, the curves in the present work are compared with both the experimental curves and these two recrystallization data points. Scatter is indicated, in part, by the degree of coincidence between these points and the experimental curves.

C. *Elastic Modulus*

An important part of the constitutive model in Eqs. [1] and [2] is the elastic modulus at the high temperatures of interest. Uncertainty exists concerning the true value of E at high temperatures.[36] This is partly because some experimental methods allow time for some creep to occur during the test, which leads to smaller estimates of the elastic modulus. In the present work, the following relation, based on experimental data from Mizukami *et al.*[37] under continuous casting conditions, was used to calculate E:

$$E[\text{GPa}] = 968 - 2.33\,(T - 273) + 1.90 \times 10^{-3}\,(T - 273)^2 - 5.18 \times 10^{-7}\,(T - 273)^3 \qquad [12]$$

where T is the temperature of interest in Kelvin. This relation applies to temperatures between 900 °C and the liquidus. The E values produced by this equation are in agreement with data reported by Patel,[38] but they are much lower than data obtained with no creep relaxation, such as those surveyed by Wray.[36]

The effect of elastic modulus on the shape of a typical calculated stress-strain curve is shown in Figure 1. Values of E were chosen by perturbing the nominal value of 14.5 GPa to encompass the wide range of data that has been reported by previous workers. Equations [1], [2], and [7] were then integrated under typical tensile test conditions at 1100 °C using the parameters of model II (Appendix II).

It is seen in Figure 1 that the elastic modulus controls the initial slope of the stress-strain curve. However, its influence diminishes with increasing strain and it has little effect beyond about 0.2 pct total strain. Considering that the experimental tensile data used to fit the inelastic parameters of the models were based on total strains of 0.1 pct or more, the value chosen for the elastic modulus would have little effect on the fitted model parameters. This implies that the elastic modulus could be varied to improve the fit at very small strains without much effect on the fit at larger strains. It was also found that numerical difficulties were fewer with a smaller elastic modulus, since the resulting size of the elastic strains, relative to the inelastic strains, is larger.

Alloy content also has a small effect on the elastic modulus. Arnoult and McLellan[39] found that at 1000 °C, the modulus decreases by 3.2 pct per wt pct carbon. In consideration of the other larger uncertainties, this dependency was not accounted for in the model.

D. *Evaluation Criteria*

Each constitutive model was evaluated according to the following criteria:

(1) Ability of the model to reproduce the experimental stress-strain curves from tensile test data and the strain-time curves from creep data over the intended range of

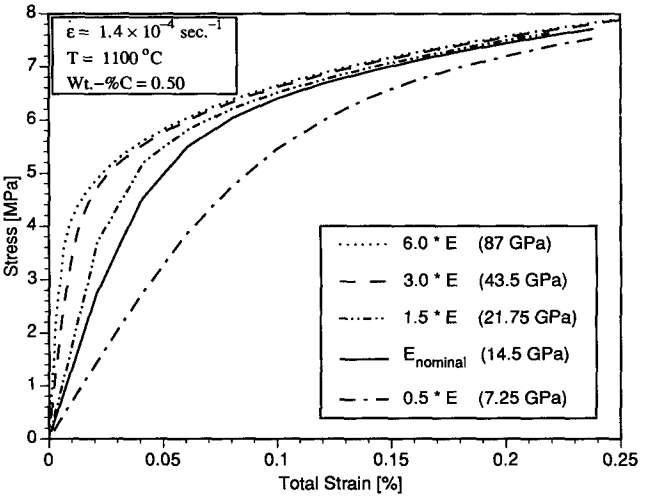

Fig. 1—Effect of variations in elastic modulus on shape of a typical stress-strain curve (model II; E_{nominal} = 14.5 GPa).

conditions. This was determined by examining the many sets of model-generated curves with the appropriate experimental data points superimposed.[30] In addition, the residual errors between the actual and predicted points were plotted against each independent variable (strain rate, temperature, carbon content, inelastic strain, and time). Trends in these plots help to identify weaknesses in the model. Finally, the absolute sum of all of the residual errors in modeling the tensile and creep data, E_1 and E_2, provided a fast indicator of the overall accuracy of each model.

(2) Ability of each model to produce qualitatively suitable behavior when modeling complex deformation histories. Several such loading conditions were examined: sudden changes in temperature, sudden changes in total strain rate, stress relaxation tests, and cyclic loading with and without stress reversal.

(3) Ease of implementation of a model into FEM code and ease of integration. This is considered relative to varying conditions and susceptibility to numerical instability.

(4) Ease of finding the "best-fit" model parameters. This is generally more difficult as the number of unknown parameters increases.

III. RESULTS

The first concern of any model is that it reproduces the data from which it was constructed. The following sections present each model and evaluate their ability to match the experimental tensile and creep test data. Table II summarizes the overall accuracy of the fit for all of the models, whose best-fitted parameters are given in Appendix II. This table provides the total error in the predicted values of the 513 tensile data points and 77 creep data points used to develop the models.

A. *Model I*

The first constitutive equation model expresses the inelastic strain rate as a function of only stress, temperature, and carbon content. Physically, this simple relation assumes that the material structure remains constant throughout the deformation process. This is characteristic of mechanical behavior in secondary or steady-state creep. This formulation has the advantage of simplicity, is easy to integrate, and has been used in several previous continuous casting bulging analyses.[22,23,27] The three specific forms used in the present work are given below,

Table II. Total Residual Errors Obtained for Each Model

Model	Tensile Error E_1 $(MPa)^2$	Creep Error E_2 $(Pct\ m/m)^2$	Total Error
IA	9733	323	13,323
IB	16,481	73	17,287
IC	12,118	43	12,595
II	1050	29	1375
III	2552	54	3150
IV	1042	33	1414

and the best estimates of the parameters, as found using the simplex method, are given in Appendix II.

$$\text{IA:}\quad \dot{\varepsilon}_p = C \exp\left(\frac{-Q}{T}\right) \sigma^n \qquad [13]$$

$$\text{IB:}\quad \dot{\varepsilon}_p = C \exp\left(\frac{-Q}{T}\right) \sinh\{a_\sigma \sigma\} \qquad [14]$$

$$\text{IC:}\quad \dot{\varepsilon}_p = C \exp\left(\frac{-Q}{T}\right) [\sinh\{a_\sigma \sigma\}]^n \qquad [15]$$

Models IA through IC differ from commonly used models[22,23,27] only by the dependence on carbon content, through factor C, and the temperature dependence of the net stress exponent, n.

Figure 2 shows how typical stress-inelastic strain curves calculated under tensile-test conditions (or "tensile curves") for model IA at different temperatures compare with the appropriate experimental data.[32] All of the tensile curves calculated for models IA through IC exhibit this same behavior of quickly reaching a flat asymptote. This is because hardening is assumed to depend only upon stress (or elastic strain). The lack of inelastic strain hardening, which is implicit in these models, is obviously a very crude approximation of the true behavior of steel over this range of conditions. This relation is naturally best at very low strain rates and/or high temperatures, where the inelastic strain rate equals the total strain rate and the plastic portion of the curve is flatter. The same conclusions apply to the tensile curves of models IB and IC which have the same flat shape but with a quantitatively worse fit (Table II).

Figure 3 shows the strain-time curves calculated for models IA and IC at 1350 °C under creep test conditions. The model-generated curves are compared with both the experimentally based curves and the recrystallization data points from Suzuki *et al.*[33] All of the calculated curves exhibit a constant slope, characteristic of the secondary

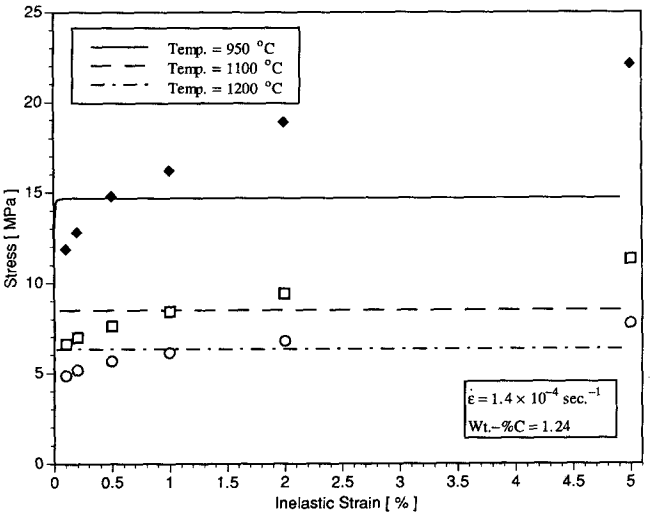

Fig. 2—Tensile test stress-strain curves calculated with model IA at different temperatures (compared with experimental tensile test data from Wray[32]).

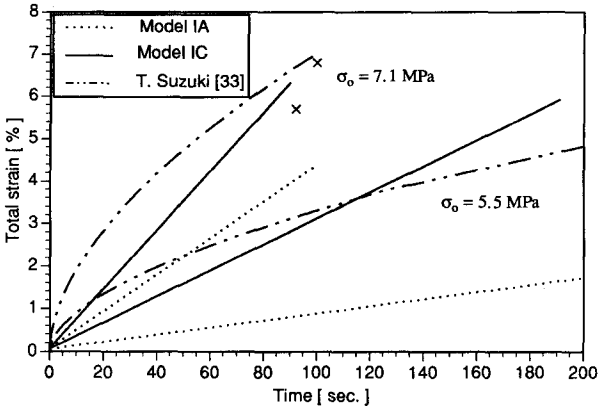

Fig. 3—Creep test strain-time curves at 1350 °C for models IA and IC (compared with experimental creep test data from Suzuki,[33] where *X* denotes recrystallization during 7.1 MPa tests).

creep assumption of these models. Neglecting primary creep, which is dominant at the low strains important to casting, results in a poor prediction of the strain. Model IA best reproduced the steady-state creep rate at large times. However, model IC matched the average creep strain better than IA for the shorter times of most interest. The creep curves for IB were similar to IC but had a slightly worse fit.

All of models IA through IC are quite crude, since they are incapable of producing the work hardening or primary creep observed in steels during casting. They might be useful only as first approximations at very high temperatures and low strain rates or stresses.

B. *Model II*

The simplest enhancement to model I is to add "time hardening." This assumes that structure evolves monotonically with increasing time since the start of the test. It provides a simple numerical mechanism to incorporate structure evolution, since time is always known during a simulation. This model therefore is just as easy as model I to integrate (for the same net stress exponent). A simple model of this form was developed from test data by Palmaers[40] and subsequently has been used successfully by several researchers to predict bulging in the continuous casting process.[23,24,25] Again, the present formulation enhances the simple form by including variation in carbon content and temperature-dependent exponents.

$$\text{II:}\quad \dot{\varepsilon}_p = C \exp\left(\frac{-Q}{T}\right) \sigma^n t^m \qquad [16]$$

The best values of the fitted parameters are given in Appendix II. It is expected that the fitted Arhennius temperature parameter, Q (~17,000 K^{-1}) should roughly compare with the activation energy for self-diffusion of austenite iron, which is about 34,000 K^{-1} (based on 284 kJ/mol and R = 8.31 J/mol K).[41] It is also interesting to note that the net stress exponent, n, always has a value near 3, which has been suggested to be the theoretically appropriate exponent for power-law creep.[42,43,44] The time exponent, m, ranges from −0.25 and −0.69, which corresponds to a value of −0.67 found by Feltham.[45]

Under tensile test conditions (constant strain rate) at significant strains, this model is equivalent to a simple strain-hardening model, such as used by Garcarz *et al.*,[46] since $\varepsilon_p/\dot{\varepsilon}_p$ can be substituted for time:

$$\dot{\varepsilon}_p = C^{1/(m+1)} \exp\left(\frac{-Q}{(m+1)\,T}\right) \sigma^{n/(m+1)}\, \varepsilon_p^{m/(m+1)} \qquad [17]$$

The form in Eq. [16] was chosen in the present work because it was found to perform better under creep conditions. In addition, it is significantly easier to integrate, since the net stress exponent n is always much smaller than $n/(m+1)$.

Representative tensile curves generated with model II are shown in Figures 4 and 5. Figure 4 shows that this model characterizes variations in temperature reasonably well, particularly at higher temperatures. This demonstrates the well-known suitability of the Arrenhius relationship for temperature-dependent effects. Figure 5 shows that wide variations in the strain rate are also well modelled with time hardening. However, time always increases during the analysis, so the model is unable to simulate constant structure. This deficiency can be seen to worsen the fit slightly at very low strain rate. Examination of the stress-inelastic strain curves also revealed that this model reproduced the tensile test data better than the model proposed by Palmaers.[40]

Figures 6 and 7 show representative creep curves at 1300 °C and 1400 °C. These figures show how model II can reasonably reproduce creep test behavior before recrystallization at temperatures below 1400 °C. At 1400 °C, the experimental strain is significantly underpredicted. The slope of the strain-time curve increases greatly with applied load, as it should. Note that there is always some curvature to these curves, since this model characterizes primary creep only. However, recrystallization usually occurs before steady-state creep is reached, so this is not a significant limitation.

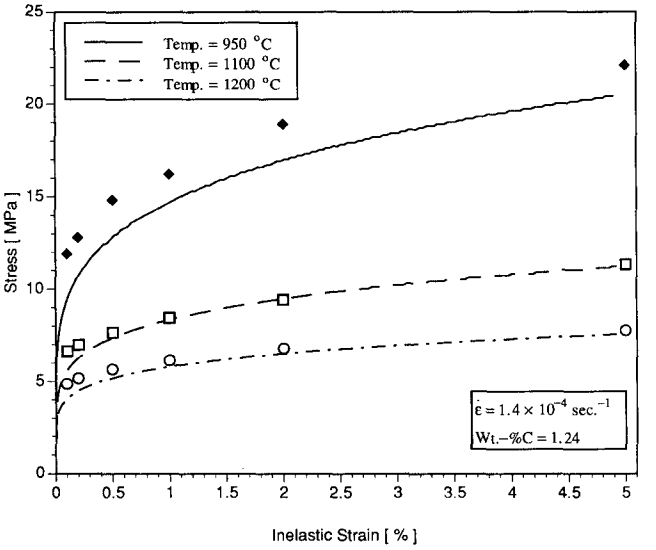

Fig. 4—Effect of temperature on tensile test curves calculated with model II (compared with Wray data[32]).

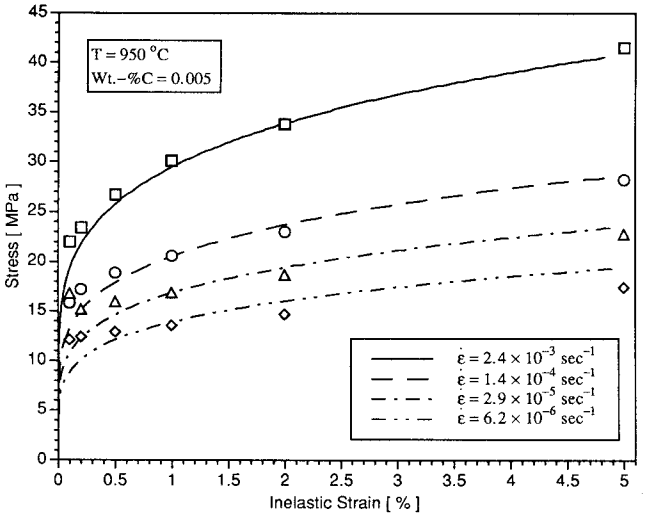

Fig. 5—Effect of strain rate on stress-strain curves calculated with model II (compared with Wray tensile data[32]).

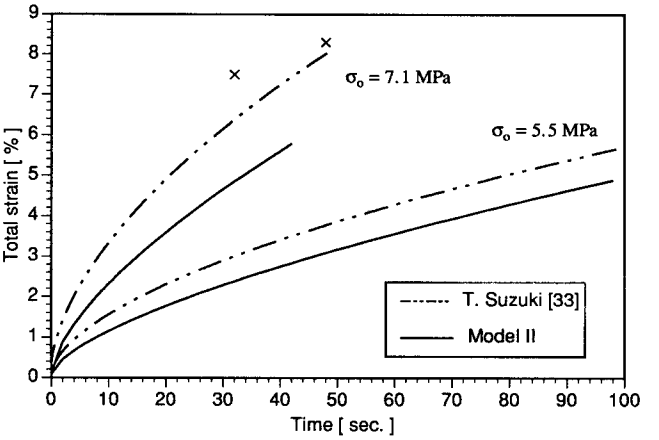

Fig. 7—Creep test curves using model II at 1400 °C (compared with Suzuki data;[33] *X* denotes recrystallization).

C. *Model III*

Model III characterizes structure evolution solely through the inelastic strain, ε_p. Numerically, evaluating this model[33] is more difficult than the previous models. However, the inelastic strain must be computed for any stress analysis, so this presents little additional difficulties to FEM implementation.

The form of model III is similar to model IA, except that the deformation rate is driven by the difference between the applied stress, σ, and a new inelastic strain term, $a_\varepsilon \varepsilon_p^{n_\varepsilon}$.

$$\text{III:} \quad \dot{\varepsilon}_p = C \exp\left(\frac{-Q}{T}\right)[\sigma - a_\varepsilon \varepsilon_p^{n_\varepsilon}]^n \qquad [18]$$

This new term is a form of "back stress" hardening parameter which has been used in previous constitutive models.[43,47] It is a highly temperature-dependent function of the inelastic strain and physically represents the threshold stress level needed to move dislocations through the current microstructure and produce permanent positive deformation. Because this back stress term evolves with inelastic strain, it introduces a temperature-dependent slope and curvature into the calculated stress-strain curves. The slope of the curve increases with increasing values of a_ε. The parameters C, n_ε, and n act in a similar manner. As their values increase, the entire plastic portion of the curve is lowered, while the slope is unaffected. This form of constitutive equation was found to produce a better fit with experimental data than other similar forms investigated. Its special attributes during complex loading will be revealed later.

Although the shapes of the curves are not exactly reproduced, the fit achieved by this model is acceptable, particularly at small strains. Table II shows that the overall fit of model III is not quite as good as Model II. Representative tensile curves calculated using this model are given in Figures 8 through 10.

Figure 8 shows how well the simple carbon-dependent factor, C, used in this model accounts for the variation in mechanical behavior with carbon content. Although similar curves for models I, II, and IV are not given,

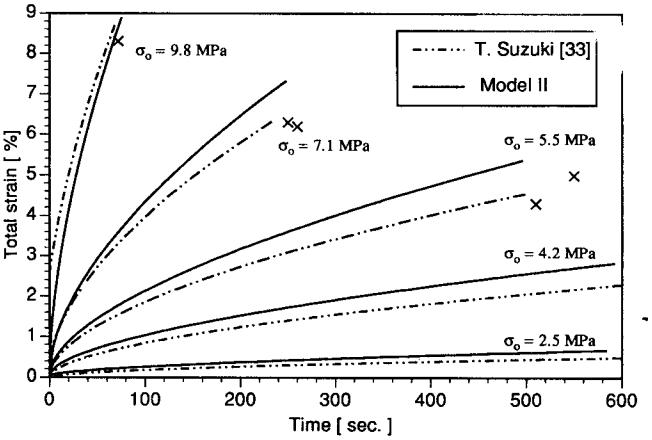

Fig. 6—Effect of stress on creep test strain-time response of model II at 1300 °C (compared with Suzuki data;[33] *X* denotes recrystallization).

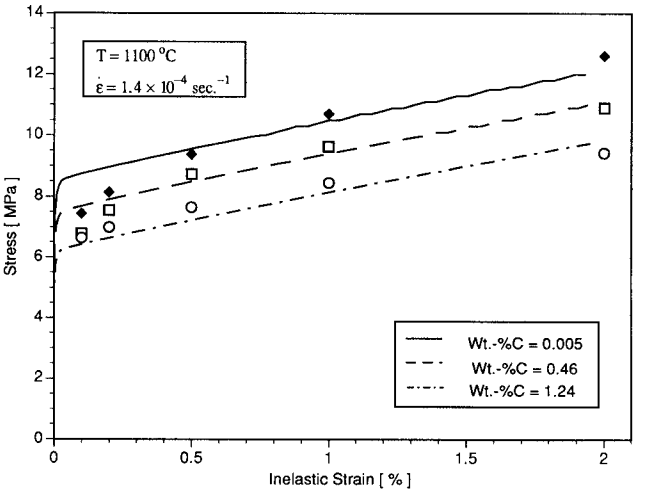

Fig. 8—Tensile test curves calculated with model III at different carbon contents (compared with Wray data[32]).

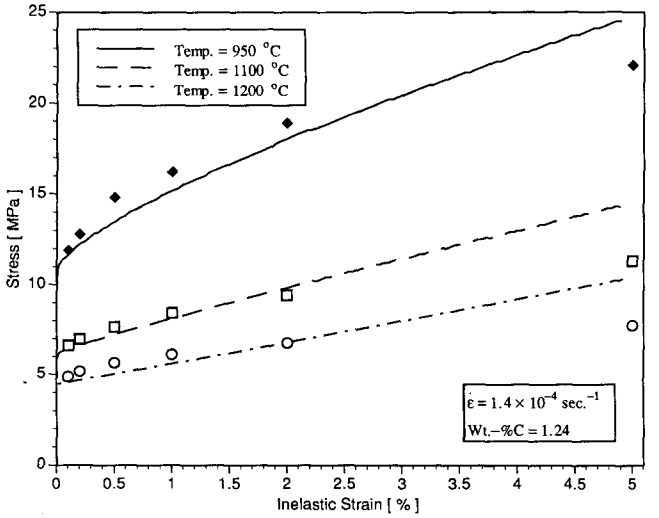

Fig. 9—Tensile test curves calculated with model III at different temperatures (compared with Wray data[32]).

they exhibit similar fit. The fit is tolerable at strains between 0.5 and 2 pct, but there are discrepancies at very small strains (below 0.2 pct). This is mainly because all of the steels have very similar initial behavior. The 0.051 pct C steel had the worst fit, particularly at very small strains. This might be due to inherent differences in the properties of steel below 0.1 pct C, which would render the simple quadratic function used in C insufficient. Differences in the initial state of those particular specimens are another possibility.

Figure 9 shows that model III can reasonably accommodate variations in temperature at small strains. Figure 10 shows that this model is able to characterize strain-rate variations only to a limited extent. This inaccuracy stems from the inability of this model formulation to change the slope of the integrated stress-strain curve as a function of strain rate. This deficiency in model III is inherent in the assumption that structure is linked to inelastic strain alone. The data show that the slope should increase significantly at higher strain rates. Fortunately, this inaccuracy is less noticeable at strains less than 2 pct, which are the most important to casting.

An example of the residual error distribution plots is given in Figure 11. Here, the difference between the predicted and experimental stress is plotted against the inelastic strain. The nonrandom trends in this plot indicate deficiencies in the model. The most serious deficiency is the constant slope of the stress-strain curves required at all strain rates. The fitted compromise is naturally best at intermediate strains and strain rates. The worst residuals are seen at large strains. This is also partly due to the inherent increase in stress level with increasing strain. The large residuals seen at strains below 0.2 pct are also partly due to the anomalous behavior of the 0.051 pct C steel. Plots of the residuals against temperature and carbon content are randomly distributed. This is consistent with the reasonable characterization with respect to those variables seen in Figures 10 and 11.

Representative creep curves for this model are shown in Figure 12 at 1300 °C. This figure illustrates that model III, like model II, can reproduce only primary creep behavior. At long times, when the inelastic strain rate approaches the total strain rate, the calculated inelastic strain approaches an asymptote, since all of the variables in Eq. [17] are then constant. Thus, model III cannot simulate steady-state creep and so has an inherent underprediction of strain at long times (relative to the stress level). This is also consistent with its poor ability to reproduce the flat tensile curves at high temperatures and low strain rates. However, Figure 12 shows that this model does produce acceptable behavior at small strains and short times.

D. *Model IV*

The final form of constitutive equation investigated uses both inelastic strain and time to characterize the structure. It is much more difficult to integrate than the

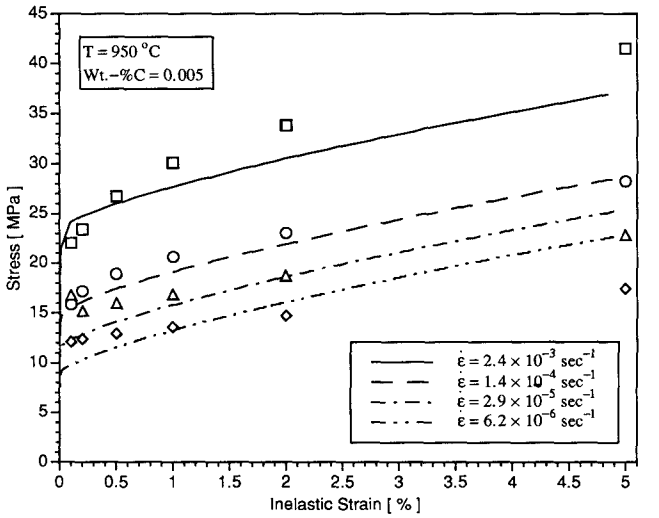

Fig. 10—Tensile test curves calculated with model III at different strain rates (compared with Wray data[32]).

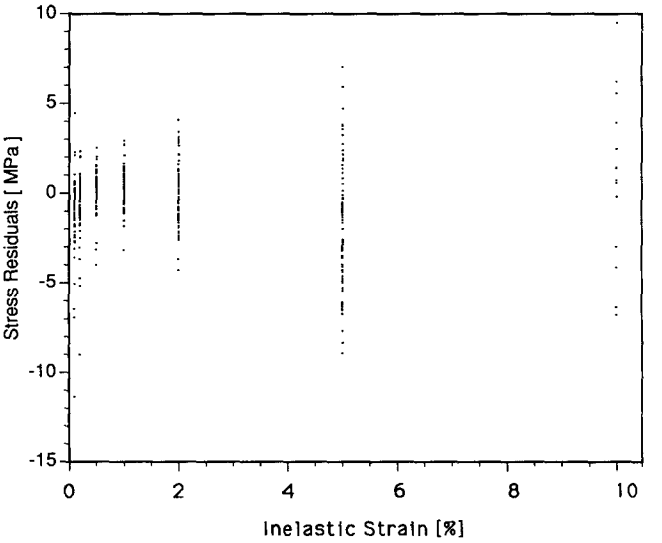

Fig. 11—Distribution of errors in model III stress predictions plotted against inelastic strain.

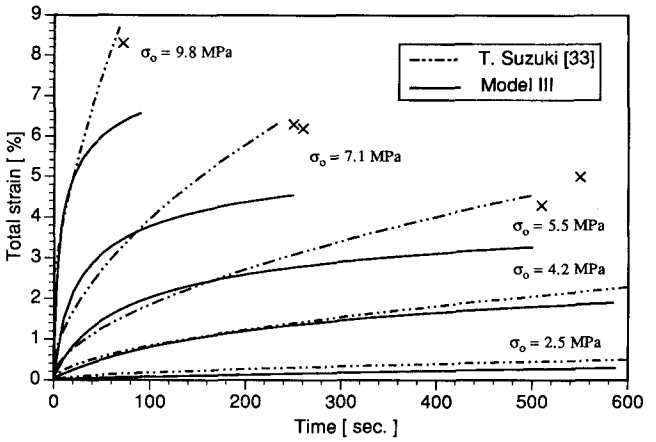

Fig. 12—Creep test curves calculated with model III at 1300 °C (compared with Suzuki[33] data; *X* denotes recrystallization).

previous models but is still relatively stable and easy to implement into existing FEM codes.

$$\text{IV:}\quad \dot{\varepsilon}_p = C \exp\left(\frac{-Q}{T}\right)[\sigma - a_\varepsilon \varepsilon_p^{n_\varepsilon} + a_t t^{n_t} \sigma^{n_\sigma}]^n \quad [19]$$

This constitutive equation differs from model III by including a time-dependent term, $a_t t^{n_t} \sigma^{n_\sigma}$, to explicitly model the phenomenon of recovery which occurs continuously during every test. This softening process reduces the slope of the stress-strain curves by annihilating dislocations that are formed *via* work hardening. This new term is also dependent on temperature, since recovery is a diffusion-controlled process, and stress, which provides a higher driving force. The qualitative effect of this term is to change the slope and curvature of the stress-strain curves with varying strain rate due to its explicit time dependence. It was expected to produce a significant improvement in fit and behavior.

Figures 13 and 14 illustrate the ability of this relation to characterize tensile test behavior. The overall fit is

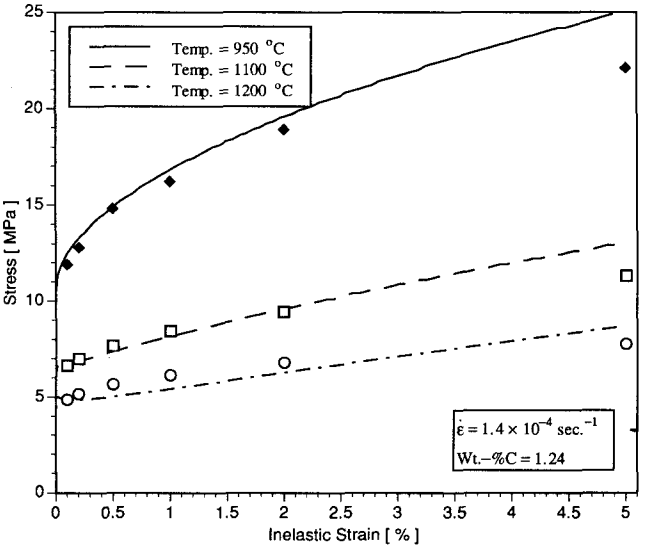

Fig. 13—Tensile test curves calculated with model IV at different temperatures (compared with Wray data[32]).

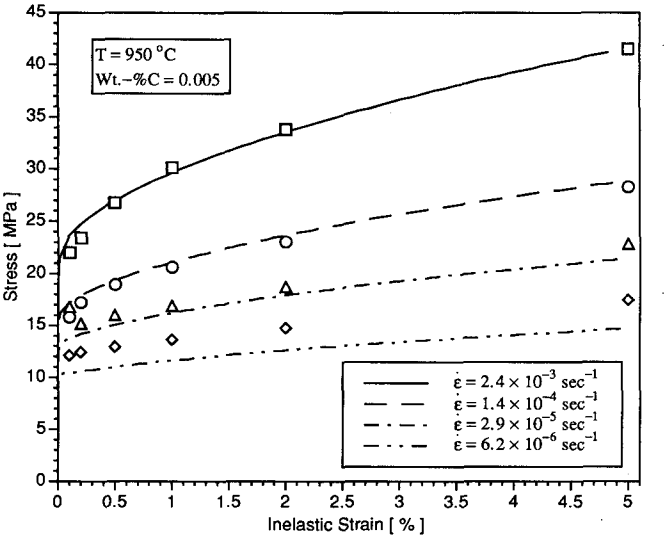

Fig. 14—Tensile test curves calculated with model IV at different strain rates (compared with Wray data[32]).

better than model III, as expected and indicated in Table II. In particular, Figure 14 shows that this model characterizes the variations in strain rate which model III had problems with.

The creep curves for model IV have the same shape as those of model III. Model IV's creep curves also approach a creep strain asymptote and, hence, are poor at long times and high temperatures. Quantitatively, however, the curves match the creep data closer than those of model III.

IV. COMPARISON WITH OTHER MEASUREMENTS

The models were run to duplicate conditions of tensile tests by Suzuki[35] on 0.25 pct C steel. A sample of the model predictions compared with the experimental data is given in Figure 15. The predicted curves are all significantly lower. This most likely is due to differences in the initial structure of the samples caused by the different annealing procedures used by Suzuki[35] and Wray[36] Suzuki annealed samples at 1400 °C and cooled to test

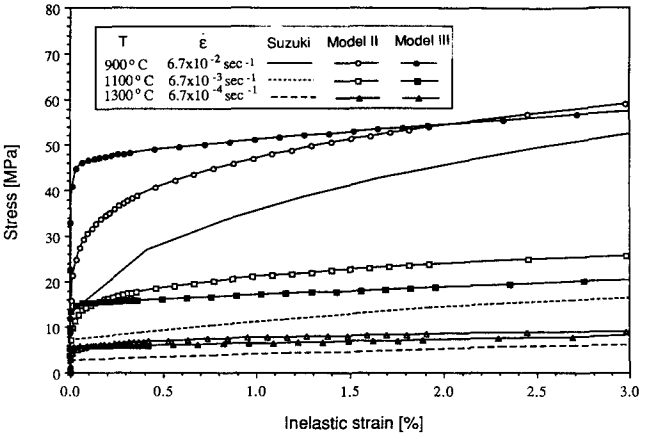

Fig. 15—Typical tensile test curves calculated with models II and III compared with Suzuki data.[35]

temperature.[35] Wray annealed samples at test temperature, which likely produced less softening and hence a stronger initial structure.

To account for this difference, the models were modified to include a normalizing factor for the initial structure. This was done by replacing stress, σ, in Eqs. [16], [18], and [19] with σ/σ_0. The "initial structure constant," σ_0, was thus always 1 for the Wray[36] tensile data and Suzuki *et al.*[33] creep data upon which the model was based. Increasing σ_0 to 1.54 for the Suzuki[35] tensile data improved the fit tremendously, as shown in Figure 16. It is surprizing that a single value for this constant produced such an improvement in fit over the entire range of temperatures and strain rates investigated. Although the fit is poor for the high strain rate data, these conditions are outside the range of interest and data used to develop the models.

The ability of the models to reasonably reproduce independent tensile test data is encouraging. However, the need for the initial structure parameter illustrates the well-known importance of sample preparation on the mechanical behavior.[35] The constitutive models should be fit to experimental data obtained from appropriately prepared samples. In the case of casting, solidifying and cooling the test specimens to the testing temperature "*in situ*" should be performed.

V. COMPLEX LOADING

The previous sections compared the performance of the various models in reproducing experimental data under standard tensile or creep test conditions. However, the conditions in continuous casting are neither constant strain rate nor constant stress. The loading in a casting process varies between these two extremes and involves continual change in temperature, stress, and strain rate over wide ranges. To evaluate the ability of each model to reproduce behavior under complex loading conditions, six different types of loading responses were investigated. These were chosen to represent extremes of the conditions actually encountered during casting.

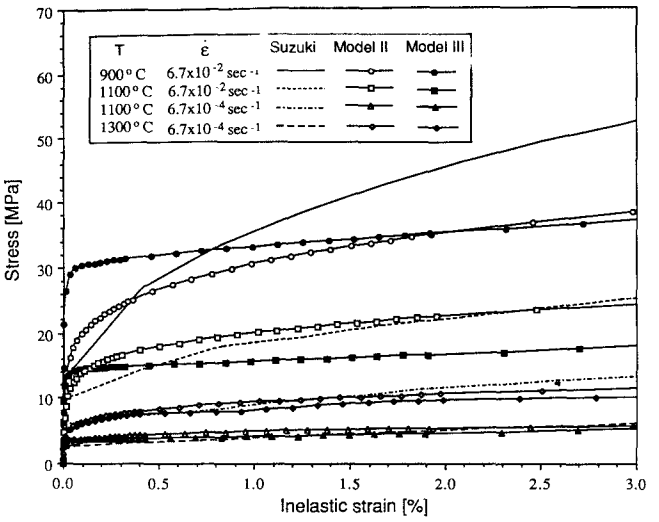

Fig. 16—Typical tensile test curves calculated with models II and III using initial structure constant of 1.54 compared with Suzuki data.[35]

A. *Sudden Temperature Changes*

The effect of suddenly decreasing the temperature during a tensile test was almost the same for all of the models investigated. The typical response is shown in Figure 17 for model II for sudden decreases in temperature from 1300 °C to 1100 °C at total strains of 1, 3, and 5 pct compared to the isothermal curves at those temperatures. The stress-strain curve is seen to follow the 1300 °C curve until the change in temperature, whereupon the stress quickly rises to join and follow the 1100 °C curve. Decreasing the temperature should produce a sharp rise in the stress that monotonically increases and asymptotically approaches the upper curve from below.[48,49] The lower temperature (upper) curve continues with an increased slope, since there is less creep. All of the models do exhibit this behavior, except that the approach is very rapid. This response seems reasonable, despite the lack of experimental validation, which is difficult to perform accurately, due to the uncertainty in small thermal strains generated in the testing equipment.

B. *Sudden Strain-Rate Changes*

Figure 18 shows the calculated response of models II through IV for tensile tests that suddenly decreased the strain rate after 1 pct strain. The figure also includes the behavior at constant strain rate for the initial 2.0×10^{-4} s^{-1} (the upper curves) and final strain rates 2.0×10^{-6} s^{-1} (the lower curves).

The expected behavior for this test is a monotonic decrease in stress from the upper curve that asymptotically approaches the lower curve from above.[48,49] This is the behavior exhibited by model IV, although the response time is rather slow. Model III simply "jumps" very rapidly between its two curves.

The response of model II is the least reasonable. Its decrement curve in Figure 18 drops below the lower 2.0×10^{-6} s^{-1} curve and then asymptotically approaches this lower curve from below. This behavior simply reflects the problems that naturally arise in a purely time-hardening model when time correlates very poorly with the deformation history. The stress level achieved at high strain

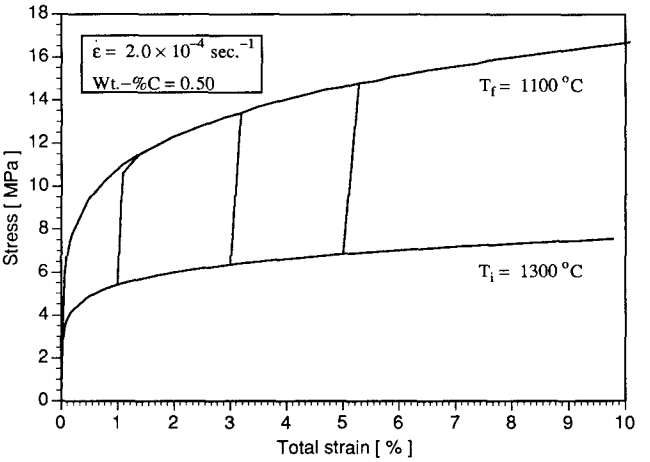

Fig. 17—Tensile test curves calculated with model II at two temperatures together with response to sudden temperature decrements at strains of 1, 3, and 5 pct.

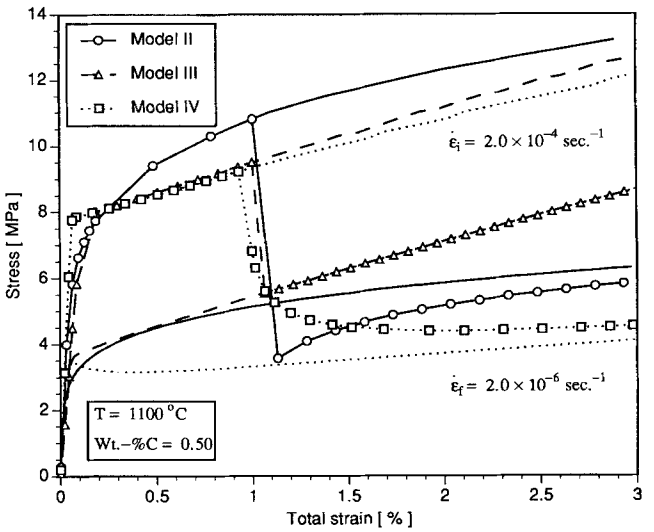

Fig. 18—Comparison of models II through IV responses to sudden decrement in strain rate at 1 pct strain together with tensile test curves calculated at the two strain rates.

rate drops suddenly to the value it would have reached at that *time* had the entire test been conducted at the current low strain rate. For example, 50 seconds of testing are required to reach 1 pct strain at the high strain rate. At the lower strain rate, 50 seconds would produce only 0.01 pct strain and a stress of 3.7 MPa. Thus, a strain-rate decrement test after 1% strain on the higher curve produces a sudden drop to about this same 3.7 MPa stress level, followed by continued reproduction of the lower strain rate curve, as if starting from 50 seconds.

Suddenly increasing the strain rate during a tensile test produced the results that would be expected based on the strain-rate decrement behavior. Model III again jumps immediately from the low strain rate curve to the high strain rate curve. Models II and IV both rise rapidly in stress and overshoot the upper curves produced from constant deformation at the high strain rate. Model II then follows a parallel path to its upper curve, but never reaching it, while Model IV asymptotically approaches its upper curve from above. Model IV also exhibited an unusual spike in each stress-strain curve at high temperatures and low strain rates due to excessive recovery. This can be seen in its lower strain rate curve in Figure 18.

Compression tests by Brown *et al.*[11] on 2 pct Si steel indicate that the response time to reach the new steady-state flow curve after a sudden increase in strain rate is very fast at these low strain rates and high temperatures. For example, the 2×10^{-3} s^{-1} flow curve was reached within about 0.5 pct strain after suddenly jumping 10 times from 2×10^{-4} s^{-1} after 10 pct strain at 800 °C.[11] Even less strain was needed at higher temperatures (1000 °C). Moreover, no overshoot in stress can be detected in these results,[11] even when jumping several orders of magnitude in strain rate. This fast response observed by Brown *et al.*[11] is consistent with the predictions of other models.[10]

Based on these experimental findings, model III appears to exhibit the most realistic response to sudden changes in strain rate, since it always "jumps" between curves very rapidly. Model IV exhibits the correct asymptotic behavior but with a slower response time than expected. Model II is the most deficient in this test, with its qualitatively unnatural response. However, the quantitative discrepancy for a sudden, two order of magnitude decrement in strain rate is not excessive, so model II might still be useful for many real processing conditions.

C. *Unload/Reload Testing*

This test is simply an extreme case of the strain-rate decrement and increment tests. The responses of models III and IV are similar to the previous test. However, the response of model II depends upon how time is treated during the reloading. Figure 19 shows a monotonic tensile curve together with two cases of unloading and reloading after 0.2 pct strain. In one case, the time, representing the hardening parameter defining the structure for this model, was "reset" to zero at the time of reloading. This reloading curve is then identical to the initial loading curve but offset by the 0.2 pct strain. In the other, "no reset" case, time was allowed to progress continuously through the test. In this case, the approach to the original curve is faster, which is the expected behavior in the absence of recrystallization. Thus, it appears that resetting the structure parameter is not appropriate until recrystallization has occurred.

D. *Stress Relaxation Tests*

Stress relaxation test conditions were chosen to duplicate tensile tests performed by Maehara *et al.* on plain 0.18 pct C steel.[28] First, monotonic loading was imposed at a constant slow strain rate to 1 pct strain. Then, the total strain was fixed (by setting the total strain rate to zero) and the stress was allowed to relax for 180 seconds due to creep. These steps were repeated several times with the application of additional loads to increase strain by 1 pct in each step. Figure 20 compares the stress-time curves calculated using models II through IV with the measured stress relaxation curve at 900 °C.

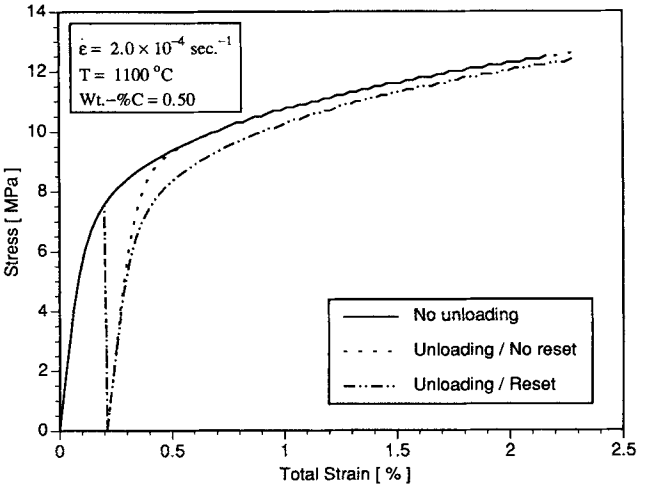

Fig. 19—Tensile test curves calculated with model II for unloading at 0.2 pct strain and reloading at the previous strain rate.

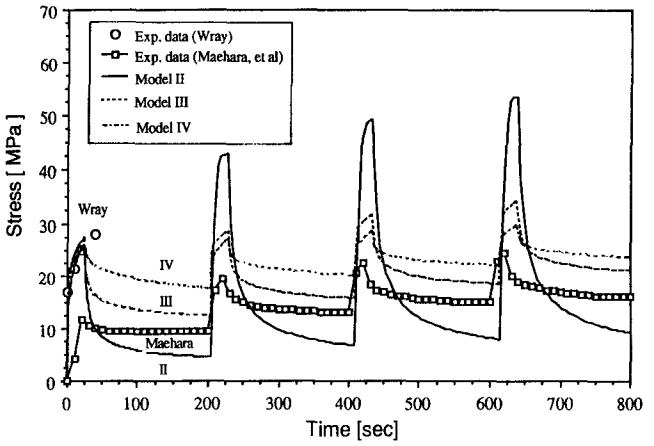

Fig. 20—Stress relaxation test response of models II through IV compared with experimental data[28] (total strain fixed after loading 0.18 pct C steel to 1 pct strain increments at 4.0×10^{-4} at 900 °C).

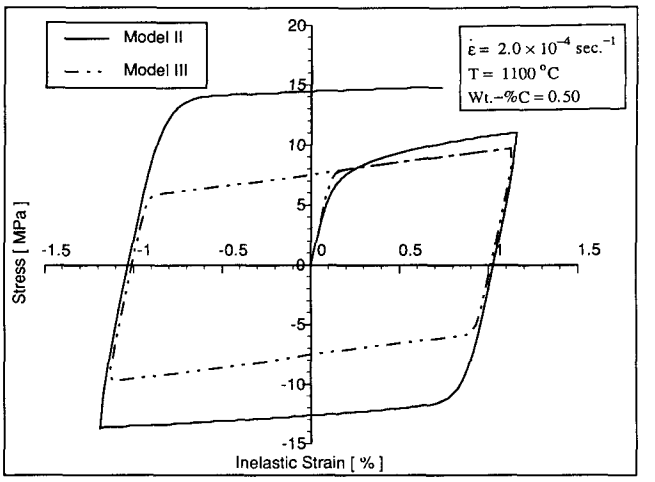

Fig. 21—Cyclic loading response of models II and III with ±1.2 pct strain cycles.

All three models behave in a similar manner until the point of first unloading and naturally match the experimental data of Wray,[32] upon which they were based. The peak stress predicted at 1 pct strain is much greater than the stress measured by Maehara *et al.*,[28] which reveals significant differences between the two sets of experimental data. Maehara *et al.* report an experimental problem of unaccounted thermal strains in the testing system, due to temperature inhomogeneity,[28] which might explain this discrepancy. Alternatively, the initial structure of the specimens may have been different, due to differences in annealing procedure prior to testing.

The subsequent relaxation behavior differs greatly in magnitude between the models. Model II produces very rapid relaxation, and without reloading, the stress would have asymptotically approached zero. Models III and IV produce slower relaxation toward a nonzero asymptote, which, for model III, is given by

$$\sigma = a_\varepsilon \varepsilon^{n_\varepsilon} \qquad [20]$$

Due to the inherent differences between the data of Wray[36] and Maehara, *et al.*[28] the stresses predicted by the models generally overestimate the Maehara measurements throughout the loading/relaxation cycles. However, the qualitative behavior is reasonable. The predicted stress drops due to relaxation by an average of 44 pct in each cycle for model III and 27 pct for model IV, which are similar to the average measured drop of 32 pct. Model II predicts an average drop of 83 pct and produces extreme increases in stress upon reloading, which is less realistic. The curve predicted by model III is the closest to the measured curve. Changing the initial structure constant to 1.4 resulted in the experimental curves consistently lying between the predicted curves of models III and IV throughout time and strain.

E. *Cyclic Loading with Stress Reversal*

The stress-strain responses of models II and III to cyclic loading conditions are shown in Figure 21. These curves were produced by reversing the strain rate whenever ±1.2 pct strain was reached. The stress predicted by the time-hardening model II is naturally seen to increase continuously as time progresses (with no reset). This is very different from the stable cyclic behavior exhibited by model III. Since model III depends on strain alone to characterize the material structure, an identical stress is produced at the corresponding strain points in each cycle. Models II and III therefore produce two possible extremes of material behavior. The long time response of model III is probably more reasonable.

Cyclic predictions for model IV are not presented since problems were encountered during the solution. This is typical of more complicated models. With further work and more experimental data, it is expected that a form of model IV should produce behavior superior to the other models. Currently, there is not enough data to characterize the behavior of steel during stress reversals at these temperatures and strains.

F. *Sinusoidal Loading without Stress Reversal*

The final loading condition investigated was monotonic, sinusoidal tensile loading, with stress variations between 0.4 and 7.0 MPa. Figure 22 compares the strain time responses of models II through IV to experimental measurements from Suzuki *et al.* for 0.19 pct C steel.[33] The degree of scatter in the measurements is indicated by error bars in the figure. All three models exhibit reasonable behavior, with model III having the best quantitative fit.

This loading case was also used to examine the potential of these models to characterize the drastic changes in microstructure and mechanical behavior that accompany recrystallization. Recrystallization was observed to occur at about 800 seconds during the experiment.[33] At this time during the simulations, the structural parameters (strain and time) were reset to zero in each model. The same expected response of increased deformation rate resulted in all of the models and the experiment. Thus, at the low strain rates encountered in casting, it appears reasonable to characterize recrystallization as a return to the initial structure. This is easily incorporated into the constitutive models, provided a function to predict the conditions for recrystallization can be developed.

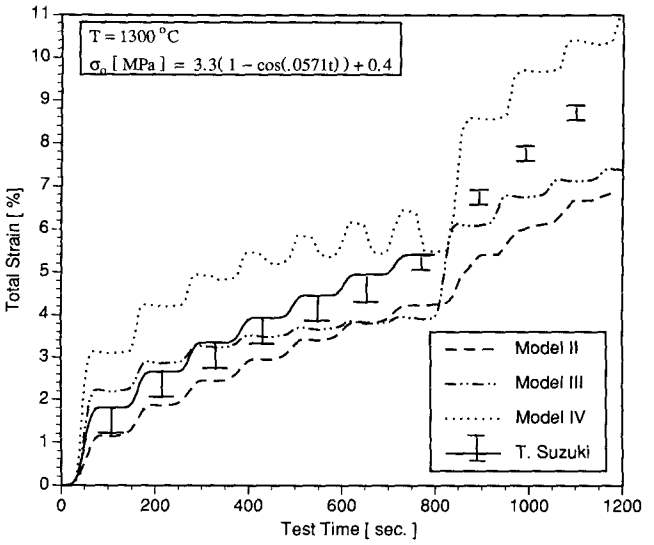

Fig. 22—Sinusoidal loading response of models II through IV compared with experimental data for 0.19 pct C steel,[33] whose range is indicated by I bars.

VI. DISCUSSION

The four different elasto-viscoplastic constitutive models have been compared over a range of common conditions. They are now evaluated together according to the criteria presented previously.

A. *Fit to Experimental Data*

None of the models tested completely fit all of the original experimental data used in their construction. However, all of the models, except model I, appear to have potential. The simplest, constant-structure models IA through IC are very crude. For the small strains important to casting processes, primary creep is dominant. Model II is always better and involves the same computational effort.

Model II had the best overall fit to the experimental data. Model III had problems at strains greater than 2 pct due to its inability to reproduce variations in the slope of the stress-strain curve for varying strain rate. Difficulties were also seen in the creep tests at long times for the same reason. However, at lower strains and times, model III was almost as accurate as models II and IV. The small strains are most important, since casting processes do not produce large strains. Furthermore, steel at high temperature can withstand only a small amount of deformation (usually 5 pct strain or less at slow strain rates) before it undergoes the drastic structural change of recrystallization. Despite its added complexity, model IV was no better than model II.

None of the models are very effective at modeling creep for long periods of time. In continuous casting, however, this is not a severe limitation, since drastic loading changes usually occur before much time elapses. The time interval between stress reversals caused by passing beneath individual support rolls and volume changes due to phase transformations is usually less than 100 seconds.

All of the models greatly underpredict the experimental creep strain at 1400 °C, while at lower temperatures, the predicted strain is usually slightly high. It is interesting to speculate that phase transformation may have occurred during those tests, since the delta-ferrite to austenite transformation temperature is 1394 °C. Phase transformations are accompanied by large amounts of inelastic strain, which increase in proportion to the stress level.[50] In addition, the creep rate of the body-centered-cubic (bcc) ferrite structure of both alpha and delta ferrite is many times higher than that of face-centered-cubic (fcc) austenite. This might explain the inability of single-phase models to achieve a reasonable fit at this temperature or higher.

To extend the valid temperature range of these constitutive models beyond austenite, relations must first be developed for single-phase alpha and delta ferrite. Then, a simple mixture rule should be able to predict the weighted average inelastic strain rate of the material, based on the volume fraction of the different phases present at that temperature.[51] In addition, an extra term might be added to Eq. [2] to account for the phenomenon of phase transformation plasticity.[52]

B. *Complex Loading*

Models II through IV all exhibit a similar ability to reasonably reproduce the experimental tensile and creep data for small strains and times. For sudden changes in temperature, the models again all behave in the same reasonable manner, jumping rapidly between curves. However, the models differ greatly in their response to complex loading conditions, including sudden changes in the strain rate, unload/reload, stress relaxation, cyclic, and sinusoidal tests.

Generally, models III and IV produced similar behavior, while model II had a more extreme, anomalous response. Using time to characterize the material structure has severe limitations when there are drastic changes in loading conditions, such as stress reversals from tension to compression. This explains the problems that model II has in reproducing complex deformation histories. Careful resetting of the time parameter to zero after severe loading reversals might extend the ability of this model.

Model III, which characterizes structure using inelastic strain, appears to have the best ability to match the experimental response to changes in strain rate, stress relaxation, and cyclic loading tests. This suggests that inelastic strain is a better parameter to characterize the material structure during complex loading histories than time. Model IV also appeared to have good potential for modeling complex loading conditions. Having both the time and inelastic strain-hardening parameters gives model IV superior qualitative ability to reproduce complex loading behavior. However, without including complex loading data when evaluating the model constants, this model is no better and may even be worse than model III. The best model, however, is still uncertain in the absence of additional experimental data. It is also unknown if these differences are important for the mechanical deformation histories of real casting processes.

C. *Numerical Stability*

The models developed in this work were all designed to be easy to implement and use in an FEM program. Models I and II are easily implemented into standard FEM creep formulations, such as used in ABAQUS.[19] Models III and IV should present few additional problems, since inelastic strain is always available and subject to convergence requirements for any simulation.

The model equations should all be easy to integrate stably for the above same reasons. However, numerical integration is easier when the exponents on simultaneously calculated variables, such as stress, are small. Larger exponents increase instability and generally require a smaller time step for integration. Model II has an advantage in this regard, since its net stress exponent is always about 3. This compares with roughly 6 for model III and 12 for model IV.

An additional important attribute of all of the models is their ability to be inverted to solve explicitly for the stress in terms of the other variables. This allows the use of alternative numerical solution strategies. Finally, a closed-form solution exists for constitutive models IA and II under some loading conditions. This can be helpful in solving the FEM stress equations and can even make numerical integration unnecessary for simple problems.

D. *Finding Model Parameters*

As the models become more complex, it is harder to find optimal values for the model parameters and to understand their meanings. In order of increasing complexity, models IA through IC had 7 to 10 parameters, models II and III each had 10, and model IV had 15. The most complex model, IV, also presented convergence problems during complex loading simulations involving stress reversals.

An exception to this general guideline is the "database" model which can guarantee an exact fit at all of the experimental data points. The main challenge in this type of model is developing the multidimensional interpolation scheme between data points. There is also the danger that any errors in the database are reproduced exactly by the model.

Finally, the form of model IV appears to be nonoptimal. Alternate forms, such as the one suggested below, might produce behavior clearly superior to models II and III, with the best attributes of both.

$$\dot{\varepsilon}_p = C \exp\left(\frac{-Q}{T}\right) (\sigma - f(\varepsilon_p, T))^n t^m \qquad [21]$$

This does not appear worth the effort, however, before finding and incorporating more experimental data for complex loading conditions. Such data could easily be used in the fitting procedure presented in this work.

VII. CONCLUSIONS

In this work, four different elasto-viscoplastic constitutive models were fit to experimental tensile and creep test data using a least-squares approach to minimize the error in their integrated curves. The models were developed for plain carbon steels with 0.005 to 1.54 pct C, temperatures in the austenite range (950 °C to 1400 °C), strain rates from 10^{-3} to 10^{-6} s^{-1}, strains less than 5 pct, and short times before recrystallization occurs. The models apply to single-phase austenite, so relations for the ferrite phases, transformation plasticity, and mixture equations to handle the multiple phases should be incorporated before these equations are applied to completely model casting processes.

The models are purposely simple, so they are easy to implement into existing finite element software and present minimal numerical difficulties. Although this simplicity limits the abilities of the models, the uncertainty and differences between available experimental data appear greater. A single constant to account for differences in initial structure between different experimental data performed adequately.

Each model has both merits and deficiencies. Model III may be the best compromise, considering its acceptable fit to the test data, reasonable behavior under complex loading conditions, and numerical stability. It is planned for use in coupled finite element models to simulate the thermal/mechanical behavior of the steel strand during continuous casting in and just below the mold. This constitutive equation should reasonably model this part of the process, because it involves relatively small loads, short times, and small strains, where this model performs best. In addition, the steel is predominantly austenite throughout the process, and stresses arising above 1400 °C should be small.

Although it is less accurate under complex loading conditions, model II has the best overall fit to the original test data and might allow faster convergence with its small net stress exponent. Hence, it may be useful for preliminary simulations, particularly when the loading history changes consistently with time. Models II and III represent extremes in behavior from completely time hardening (II) to completely strain hardening (III). Thus, if the differences between process simulation results obtained using these two models is small, the importance of complex loading conditions is not important, and the results are likely to be reasonable with either model. The enhanced performance of model IV, which has both time and strain hardening, does not appear to be worth its added complexity and inferior stability at present.

More experimental data are needed to determine the true behavior of steel under complex loading conditions relevant to casting before more sophisticated models are warranted. Additional experimental data are also needed at very low strains (below 0.5 pct) for the range of steel grades cast, particularly at very high temperatures (above 1400 °C). In fitting the parameters of future models, a multiphase model incorporating transformation plasticity is recommended for data at 1400 °C and above. Additional work is also needed to quantify the conditions required for recrystallization. The results of this work suggest that simple models may be suitable for reproducing the mechanical behavior of steel during casting processes, even when complex phenomena such as recrystallization are present.

APPENDIX I

Creep test data

Temperature (°C)	Stress (MPa)	Time (s)						
		20	40	60	80	100	120	140
1250	5.5	0.4 pct ε	0.6	0.8	0.9	1.0	1.1	1.2
1250	7.1	0.9	1.3	1.6	1.8	2.1	2.3	2.6
1250	9.8	2.4	3.4	4.2	4.9	5.6	6.2	6.6
1300	4.2	0.34	0.50	0.63	0.74	0.84	0.93	1.0
1300	5.5	0.8	1.1	1.4	1.6	1.9	2.1	2.2
1300	7.1	1.7	2.4	3.0	3.5	4.0	4.3	4.4
1350	4.2	0.6	0.9	1.1	1.3	1.5	1.7	1.8
1350	5.5	1.4	2.0	2.5	2.9	3.3	3.7	4.0
1350	7.1	3.2	4.5	5.6	6.4	7.5	8.0	8.6
1400	4.2	1.1	1.6	2.0	2.3	2.6	2.9	3.1
1400	5.5	2.6	3.6	4.4	5.1	5.9	6.4	7.0

This table presents the percent strain/time data points defining the creep curves used in fitting the models. The data were obtained by integrating the equations given by Suzuki *et al.*[33] These data are consistent with the selected data included in their article.[33]

APPENDIX II

Constitutive equation summary

Model IA

$$\dot{\varepsilon}_p = C \exp\left(\frac{-Q}{T}\right) \sigma^n$$

$C = 24{,}233 + 49{,}973\ (\text{pct C}) + 48{,}757\ (\text{pct C})^2$
$Q = 49{,}480$
$n = 5.331 + 4.116 \times 10^{-3}\ T - 2.116 \times 10^{-6}\ T^2$

Model IB

$$\dot{\varepsilon}_p = C \exp\left(\frac{-Q}{T}\right) \sinh\{a_\sigma \sigma\}$$

$C = 2.602 \times 10^{10} + 2.265 \times 10^{12}\ (\text{pct C}) - 1.332 \times 10^{12}\ (\text{pct C})^2$
$Q = 56{,}423$
$n = 1.5403 + 5.913 \times 10^{-5}\ T - 5.538 - 10^{-7}\ T^2$

Model IC

$$\dot{\varepsilon}_p = C \exp\left(\frac{-Q}{T}\right) [\sinh\{a_\sigma \sigma\}]^n$$

$C = 1.802 \times 10^6 + 1.742 \times 10^8\ (\text{pct C}) - 6.503 \times 10^7\ (\text{pct C})^2$
$Q = 44{,}809$
$a_\sigma = 1.068 + 1.702 \times 10^{-4}\ T - 2.808 \times 10^{-7}\ T^2$
$n = 0.200 + 3.966 \times 10^{-4}\ T$

Model II

$$\dot{\varepsilon}_p = C \exp\left(\frac{-Q}{T}\right) \sigma^n t^m$$

$C = 0.3091 + 0.2090\ (\text{pct C}) + 0.1773\ (\text{pct C})^2$
$Q = 17{,}160$
$n = 6.365 - 4.521 \times 10^{-3}\ T + 1.439 \times 10^{-6}\ T^2$
$m = -1.362 + 5.761 \times 10^{-4}\ T + 1.982 \times 10^{-8}\ T^2$

Model III

$$\dot{\varepsilon}_p = C \exp\left(\frac{-Q}{T}\right) [\sigma - a_\varepsilon \varepsilon_p^{n_\varepsilon}]^n$$

$C = 46{,}550 + 71{,}400\ (\text{pct C}) + 12{,}000\ (\text{pct C})^2$
$Q = 44{,}650$
$a_\varepsilon = 130.5 - 5.128 \times 10^{-3}\ T$
$n_\varepsilon = -0.6289 + 1.114 \times 10^{-3}\ T$
$n = 8.132 - 1.540 \times 10^{-3}\ T$

Model IV

$$\dot{\varepsilon}_p = C \exp\left(\frac{-Q}{T}\right) [\sigma - a_\varepsilon \varepsilon_p^{n_\varepsilon} + a_t t^{n_t} \sigma^{n_\sigma}]^n$$

$C = 6519 + 1.005 \times 10^5\ (\text{pct C}) + 3.664 \times 10^5\ (\text{pct C})^2$
$Q = 64{,}020$
$a_\varepsilon = 162.7 - 4.326 \times 10^{-3}\ T$
$n_\varepsilon = -1.069 + 1.345 \times 10^{-3}\ T$
$a_t = 0.1495$
$n_t = 0.3299$
$n_\sigma = 0.7224 - 9.885 \times 10^{-5}\ T + 1.541 \times 10^{-7}\ T^2$
$n = 12.81 - 6.645 \times 10^{-4}\ T$

NOMENCLATURE

Variables	Definition	Units
σ	stress	MPa
$\hat{\sigma}$	predicted value of σ	MPa
ε_e	elastic strain	m/m
ε_p	inelastic strain	m/m
ε	total strain	m/m
$\hat{\varepsilon}$	predicted value of ε	m/m
E	Young's modulus	GPa
T	temperature	Kelvin
$\dot{\sigma}$	stress rate	MPa s^{-1}
$\dot{\varepsilon}$	total strain rate	s^{-1}
$\dot{\varepsilon}_e$	elastic strain rate	s^{-1}

$\dot{\varepsilon}_p$	inelastic strain rate	s^{-1}
$\dot{\varepsilon}_T$	thermal strain rate	s^{-1}
E_1	error in fitting tensile data	MPa^2
E_2	error in fitting creep data	$(pct\ m/m)^2$
t	time	s
α_i	internal structure variable	(varies)

Model-Fitted Parameters

C	carbon content-dependent function	$MPa^{-n}\ s^{-m-1}$
Q	activation energy constant	Kelvin
σ_0	initial structure constant	—
a_σ	temperature-dependent constant	MPa^{-1}
a_t	constant in model IV	$MPa^{1-n_\sigma}\ s^{-n_t}$
a_ε	temperature-dependent constant	$MPa\ s^{-n_\varepsilon}$
a_ε	temperature-dependent constant	$MPa\ s^{-n_\varepsilon}$
m	temperature-dependent time exponent	—
n	temperature-dependent net stress exponent	—
n_ε	temperature-dependent inelastic strain exponent	—
n_σ	temperature-dependent exponent in model IV	—
n_t	time exponent in model IV	—

ACKNOWLEDGMENTS

The authors wish to thank Inland Steel, ARMCO, Inc., BHP Steel, LTV Steel, and the National Science Foundation (Grant No. MSS-8957195-PYI) for funding which made this work possible.

REFERENCES

1. A. Mendelson: *Plasticity—Theory and Applications*, R.E. Krieger Publishing, Malabar, FL, 1968 (reprinted 1983), pp. 213-15.
2. D. Owen and E. Hinton: *Finite Elements in Plasticity*, first ed., Pineridge Press Limited, Swansea, United Kingdom, 1980.
3. B.G. Thomas, I.V. Samarasekera, and J.K. Brimacombe: *Metall. Trans. B*, 1987, vol. 18B (1), pp. 131-47.
4. K. Sorimachi and J.K. Brimacombe: *Ironmaking and Steelmaking*, 1977, vol. 4, pp. 240-45.
5. M. Uehara, I.V. Samarasekera, and J.K. Brimacombe: *Ironmaking and Steelmaking*, 1986, vol. 13 (3), p. 138.
6. J.E. Kelly, K.P. Michalek, T.G. O'Connor, B.G. Thomas, and J.A. Dantzig: *Metall. Trans. A*, 1988, vol. 19A (10), pp. 2589-2602.
7. E.T. Till, R.D. Moser, R.S. Scheidl, and K.L. Schwaha: Voest-Alpine Linz, Austria, Report No. CCC 25, 1987.
8. F.G. Rammerstorfer, C. Jaquemar, D.F. Fischer, and H. Wiesinger: *Int. Conf. Numerical Methods in Thermal Problems*, R. Lewis and K. Morgan, eds., Pineridge Press Ltd., Swansea, United Kingdom, 1979, pp. 712-22.
9. A. Miller: *Unified Constitutive Equations for Creep and Plasticity*, Elsevier Applied Science Publishers Ltd., Essex, United Kingdom, 1987, pp. 1-341.
10. L. Anand: *Trans. ASME, J. Eng. Mater. Technol.*, 1982, vol. 104, pp. 12-17.
11. S. Brown, K. Kim, and L. Anand: *Int. J. Plasticity*, 1989, vol. 5 (2), pp. 95-130.
12. R.O. Adebanjo and A.K. Miller: *Mater. Sci. Eng.*, 1989, vol. A119, pp. 95-101.
13. U.S. Lindholm: *Interdisciplanary Issues in Materials Processing and Manufacturing*, ASME, New York, NY, 1987, pp. 77-93.
14. I.R. Orisamolu and M.C. Singh: *J. Thermal Stresses*, 1989, vol. 12, pp. 351-68.
15. R.E. Smelser and O. Richmond: *Modeling of Casting and Welding Processes IV*, A. Giamei and G. Abbaschian, eds., TMS, Warrendale, PA, 1988, pp. 313-28.
16. D. Bammann and R.D. Krieg: in *Unified Constitutive Equations for Creep and Plasticity*, A. Miller, ed., Elsevier Applied Science Publishers Ltd., Essex, United Kingdom, 1987, p. 325.
17. I. Cormeau: *Int. J. Numer. Methods Eng.*, 1975, vol. 9, pp. 109-27.
18. G.G. Chen and T.R. Hsu: *Int. J. Numer. Methods Eng.*, 1988, vol. 26, pp. 511-24.
19. ABAQUS: *User's Manual*, Hibbitt, Karlsson & Sorensen, Inc., Providence, RI, 1990.
20. B. Aksel: Ph.D. Thesis, Cornell University, Ithaca, NY, 1990.
21. O.M. Puhringer: *Stahl Eisen*, 1976, vol. 96 (6), pp. 279-84.
22. K. Miyazawa and K. Schwerdtfeger: *Ironmaking and Steelmaking*, 1979, vol. 6 (2), pp. 68-74.
23. A. Palmaers, A. Etienne, and J. Mignon: *Stahl Eisen*, 1979, vol. 99 (19), pp. 1039-50.
24. A. Grill and K. Schwerdtfeger: *Ironmaking and Steelmaking*, 1979, vol. 6 (3), pp. 131-35.
25. B. Barber, B.A. Lewis, and B.M. Leckenby: *Iron and Steel*, 1985, vol. 12 (4), pp. 171-75.
26. J.B. Dalin and J.L. Chenot: *Int. J. Numer. Methods Eng.*, 1988, vol. 25, pp. 147-63.
27. A. Ramacciotti: *Steel Res.*, 1988, vol. 59 (10), pp. 438-48.
28. Y. Maehara, H. Tomono, and Y. Ohmori: *Trans. Iron Steel Inst. Jpn.*, 1987, vol. 27, pp. 499-505.
29. J. Azzi: Master's Thesis, University of Illinois at Urbana–Champaign, 1986.
30. P. Kozlowski: Master's Thesis, University of Illinois at Urbana–Champaign, 1991.
31. W.H. Press, B.P. Flannery, S.A. Teukolsky, and W.T. Vetterling: *Numerical Recipes*, Cambridge University Press, New York, NY, 1988, pp. 289-93.
32. P.J. Wray: *Metall. Trans. A*, 1982, vol. 13A (1), pp. 125-34.
33. T. Suzuki, K.H. Tacke, K. Wunnenberg, and K. Schwerdtfeger: *Ironmaking and Steelmaking*, 1988, vol. 15 (2), pp. 90-100.
34. F.J. Clauss: in *Engineers Guide to High Temperature Materials*, Addison-Wesley, Reading, MA, 1969, pp. 13-17.
35. H.G. Suzuki: Nippon Steel, Chiba, Japan, private communication, 1990.
36. P.J. Wray: *Modelling of Casting and Welding Processes, AIME Conf. Proc.*, Ringe, NH, 1980, pp. 245-57.
37. H. Mizukami, K. Murakami, and Y. Miyashita: *Tetsu-to-Hagané*, 1977, vol. 63 (146), p. S-652.
38. B. Patel: Ph.D. Thesis, Carleton University, Ottawa, Canada, 1985.
39. W.J. Arnoult and R.B. McLellan: *Acta Metall.*, 1975, vol. 23, pp. 51-56.
40. A. Palmaers: Centre de Recherches Metallurgiques, Liege, Belgium, Report No. 53, 1978, pp. 23-31.
41. E.A. Brandes: *Smithell's Metals Reference Book*, 6th ed., Butterworth's, Boston, 1983, pp. 13/11.
42. Z. Horita and T.G. Langdon: *Proc. 2nd Int. Conf. Creep and Fracture of Engineering Materials and Structures*, Pineridge Press, Swansea, United Kingdom, 1984, p. 75.
43. B.A. Senior: *Mater. Sci. Eng.*, 1990, vol. A124, pp. 159-69.
44. J. Weertman and J.R. Weertman: in *Physical Metallurgy*, R. Cahn, ed., North Holland, Amsterdam, 1965, p. 793.
45. P. Feltham: *Proc. Phys. Soc.*, 1953, vol. 66, pp. 865-83.
46. J. Gancarz, J.Y. Lamant, M. Larrecq, and P. Rahier: *Steelmaking Conf.*, Iron and Steel Society–AIME, Washington, DC, 1991, vol. 47.
47. D. Slavik and H. Sehitoglu: *Pressure Vessels and Piping Conf.*, H. Sehitoglu and S.Y. Zamrik, eds., ASME, San Diego, CA, 1987, vol. 123.
48. J. Klepaczko, R.A. Frantz, and J. Duffy: *Rozprawy Inzynierskie—Engineering Transactions*, 1977, vol. 25, pp. 1-22.
49. J.R. Klepaczko and C.Y. Chiem: *J. Mech. Phys. Solids*, 1986, vol. 34 (1), pp. 29-54.
50. J.B. Leblond, G. Mottet, and J.C. Devaux: *J. Mech. Phys. Solids*, 1986, vol. 34 (4), pp. 395-432.
51. P.J. Wray: *Met. Technol.*, 1981, Dec., pp. 466-71.
52. J.B. Leblond, J. Devaux, and J.C. Devaux: *Int. J. Plast.*, 1989, vol. 5 (6), pp. 551-92.